

## Influence of interfacial coherency on ferroelectric switching of superlattice BaTiO<sub>3</sub>/SrTiO<sub>3</sub>

Pingping Wu, Xingqiao Ma, Yulan Li, Chang-Beom Eom, Darrell G. Schlom, Venkatraman Gopalan, and Long-Qing Chen

Citation: *Applied Physics Letters* **107**, 122906 (2015); doi: 10.1063/1.4931129

View online: <http://dx.doi.org/10.1063/1.4931129>

View Table of Contents: <http://scitation.aip.org/content/aip/journal/apl/107/12?ver=pdfcov>

Published by the [AIP Publishing](#)

---

### Articles you may be interested in

[Tuning of dielectric, pyroelectric and ferroelectric properties of 0.715Bi0.5Na0.5TiO<sub>3</sub>-0.065BaTiO<sub>3</sub>-0.22SrTiO<sub>3</sub> ceramic by internal clamping](#)

*AIP Advances* **5**, 087145 (2015); 10.1063/1.4929328

[Insight on the ferroelectric properties in a \(BiFeO<sub>3</sub>\)<sub>2</sub>\(SrTiO<sub>3</sub>\)<sub>4</sub> superlattice from experiment and ab initio calculations](#)

*Appl. Phys. Lett.* **107**, 042904 (2015); 10.1063/1.4927600

[90-degree polarization switching in BaTiO<sub>3</sub> crystals without domain wall motion](#)

*Appl. Phys. Lett.* **103**, 232901 (2013); 10.1063/1.4832784

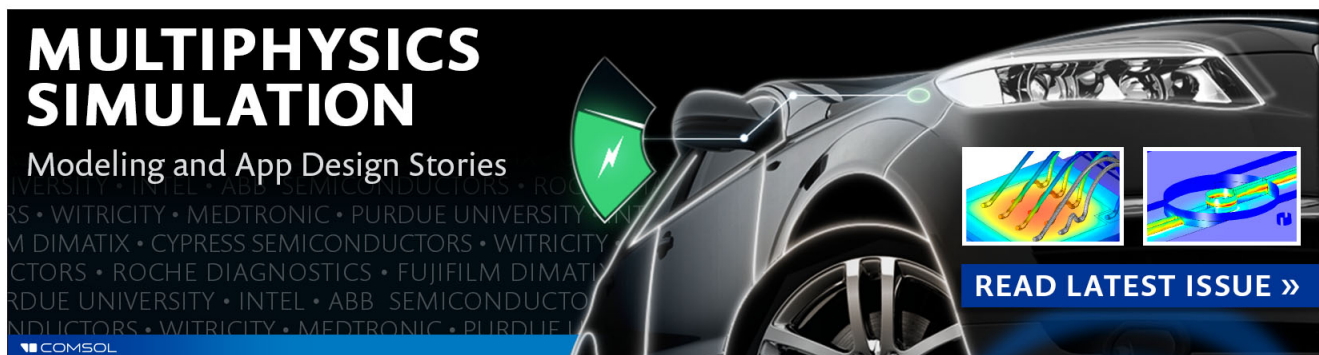
[Compositional engineering of BaTiO<sub>3</sub>/\(Ba,Sr\)TiO<sub>3</sub> ferroelectric superlattices](#)

*J. Appl. Phys.* **114**, 104102 (2013); 10.1063/1.4820576

[Dipole spring ferroelectrics in superlattice SrTiO<sub>3</sub>/BaTiO<sub>3</sub> thin films exhibiting constricted hysteresis loops](#)

*Appl. Phys. Lett.* **100**, 092905 (2012); 10.1063/1.3691172

---

The advertisement features a dark background with a car's front end on the right. On the left, the text 'MULTIPHYSICS SIMULATION' is written in large, bold, white letters. Below it, 'Modeling and App Design Stories' is written in a smaller white font. A green lightning bolt icon is positioned to the left of the car. Two small inset images show simulation results: one with a color gradient and another with a blue and yellow pattern. At the bottom left, the COMSOL logo is visible. At the bottom right, a blue button with white text says 'READ LATEST ISSUE >>'.

**MULTIPHYSICS  
SIMULATION**

Modeling and App Design Stories

UNIVERSITY • INTEL • ABB SEMICONDUCTORS • ROCH  
RS • WITRICITY • MEDTRONIC • PURDUE UNIVERSITY • IN  
M DIMATIX • CYPRESS SEMICONDUCTORS • WITRICITY  
CTORS • ROCHE DIAGNOSTICS • FUJIFILM DIMATI  
RDUE UNIVERSITY • INTEL • ABB SEMICONDUCTO  
NDUCTORS • WITRICITY • MEDTRONIC • PURDUE U

COMSOL

READ LATEST ISSUE >>

# Influence of interfacial coherency on ferroelectric switching of superlattice BaTiO<sub>3</sub>/SrTiO<sub>3</sub>

Pingping Wu,<sup>1,2</sup> Xingqiao Ma,<sup>1</sup> Yulan Li,<sup>3</sup> Chang-Beom Eom,<sup>4</sup> Darrell G. Schlom,<sup>5</sup> Venkatraman Gopalan,<sup>2</sup> and Long-Qing Chen<sup>2</sup>

<sup>1</sup>*Department of Physics, University of Science and Technology Beijing, Beijing, Beijing 100083, China*

<sup>2</sup>*Department of Materials Science and Engineering, The Pennsylvania State University, University Park, Pennsylvania 16802, USA*

<sup>3</sup>*Pacific Northwest National Laboratory, Richland, Washington 99352, USA*

<sup>4</sup>*Department of Materials Science and Engineering, University of Wisconsin Madison, Madison, Wisconsin 53706, USA*

<sup>5</sup>*Department of Materials Science and Engineering, Cornell University, Ithaca, New York 14853, USA and Kavli Institute at Cornell for Nanoscale Science, Ithaca, New York 14853, USA*

(Received 29 August 2015; accepted 6 September 2015; published online 25 September 2015)

The switching behavior of a (BaTiO<sub>3</sub>)<sub>8</sub>/(SrTiO<sub>3</sub>)<sub>4</sub> superlattice grown on a SrTiO<sub>3</sub> substrate was simulated utilizing the phase field method. To investigate the effect of the mechanical constraint of the substrate on switching, three types of superlattice/substrate interface mechanical relaxation conditions were considered: (1) fully commensurate, (2) partially relaxed, and (3) fully relaxed. Our simulation results demonstrate that the hysteresis loops under the three types of constraints are very different. The interfacial coherency dramatically affects the coercive field and remanent polarization of the superlattices. The mechanism underlying the hysteresis loop variation with interfacial coherency was investigated by analyzing the ferroelectric domain configuration and its evolution during the switching process. The simulated hysteresis loop of the fully relaxed superlattice exhibits a shape that is potentially relevant to the application of ferroelectrics for energy storage materials. © 2015 AIP Publishing LLC.

[<http://dx.doi.org/10.1063/1.4931129>]

The synthesis of oxide heterostructures with control at the atomic level has made significant progress, making it possible to customize complex periodic ferroelectric superlattices with great flexibility in stacking sequence.<sup>1–4</sup> Recently, much interest has been directed towards BaTiO<sub>3</sub>(BT)/SrTiO<sub>3</sub>(ST) superlattices due to their chemical stability and highly responsive dielectric constant.<sup>5–16</sup> Due to the presence of misfit dislocations, however, the ferroelectric behavior of the superlattices is strongly influenced by the mechanical boundary conditions between the BT/ST superlattice film and its underlying substrate. In particular, the relaxation between the thin film/substrate interface can greatly affect the ferroelectric domain structure,<sup>17</sup> phase transition temperature,<sup>18,19</sup> dielectric properties,<sup>20</sup> remanent polarization,<sup>21</sup> and the hysteresis loop of polarization vs. externally applied electric field (P-E loop).<sup>22–24</sup> Thus, it is essential to investigate the ferroelectric properties together with the domain microstructures to understand the influence of strain relaxation within BT/ST superlattices. These superlattices can be denoted by BT<sub>*n*</sub>/ST<sub>*m*</sub>, where *n* and *m* refer to the thickness, in unit cells, of the (001)<sub>*p*</sub> BaTiO<sub>3</sub> and (001)<sub>*p*</sub> SrTiO<sub>3</sub> layers, respectively, and the subscript *p* refers to the pseudocubic indices.

In this letter, a BT<sub>8</sub>/ST<sub>4</sub> superlattice grown on a (001) ST substrate is employed as our model system. The main objective of this work is to investigate the switching properties of the constrained superlattice, i.e., the P-E loop. P-E loop is a very important characteristic of ferroelectrics for its applications in electronic memory devices.<sup>25</sup> The evolution of the ferroelectric domain structure during the switching

process is, however, not easily observed; thus computational methods are extremely useful for understanding the relationship between the domain structure and the P-E hysteresis loops.<sup>26,27</sup> Superlattices have the potential to adjust their switching properties as a function of mechanical boundary conditions.<sup>28</sup> At room temperature, a SrTiO<sub>3</sub> single crystal is paraelectric and a BaTiO<sub>3</sub> single crystal is ferroelectric and shows a square-shaped hysteresis loop. Their combination either in a solid solution state or a superlattice structure reveals interesting ferroelectric properties, which have been investigated by several experimental studies<sup>28</sup> and numerical simulations.<sup>17,29–32</sup> Most work on superlattices has focused on the structure and major ferroelectric properties. The influence of structural relaxation on the switching properties of such superlattices has been less studied, except Refs. 22–24. In this work, we report our phase-field simulations of the ferroelectric hysteresis loops of BT<sub>8</sub>/ST<sub>4</sub> superlattices under fully commensurate, partially relaxed, and fully relaxed constraints. The switching process of the superlattice is illustrated and explained through the corresponding superlattice ferroelectric domain structure evolution.

In order to model a proper ferroelectric domain structure by the phase-field method, the 3-components  $P_i$  ( $i = 1, 2, 3$ ) of the spontaneous polarization are chosen as the order parameters. The equilibrium ferroelectric domain structure can be obtained by solving the time dependent Ginzburg-Landau (TDGL) equations

$$\frac{\partial P_i(x, t)}{\partial t} = -L \frac{\delta F_{total}}{\delta P_i(x, t)}, \quad (i = 1, 2, 3), \quad (1)$$

where  $L$  is the kinetic coefficient to describe domain wall mobility,  $x = (x_1, x_2, x_3)$  is the coordinate, and  $t$  is time.  $F_{total}$  is the total energy of the system under consideration and can be expressed by

$$F_{total} = F_{bulk} + F_{grad} + F_{elast} + F_{elec}, \quad (2)$$

$$\begin{aligned} F_{bulk}(P_i) = & \int_v \alpha_1(P_1^2 + P_2^2 + P_3^2) + \alpha_{11}(P_1^4 + P_2^4 + P_3^4) + \alpha_{12}(P_1^2P_2^2 + P_1^2P_3^2 + P_2^2P_3^2) + \alpha_{111}(P_1^6 + P_2^6 + P_3^6) \\ & + \alpha_{112}[P_1^2(P_2^4 + P_3^4) + P_2^2(P_1^4 + P_3^4) + P_3^2(P_1^4 + P_2^4)] + \alpha_{123}P_1^2P_2^2P_3^2 + \alpha_{1111}(P_1^8 + P_2^8 + P_3^8) \\ & + \alpha_{1112}[P_1^6(P_2^2 + P_3^2) + P_2^6(P_1^2 + P_3^2) + P_3^6(P_1^2 + P_2^2)] + \alpha_{1122}(P_1^4P_2^4 + P_1^4P_3^4 + P_2^4P_3^4) \\ & + \alpha_{1123}(P_1^4P_2^2P_3^2 + P_2^4P_1^2P_3^2 + P_3^4P_1^2P_2^2)d^3x, \end{aligned} \quad (3)$$

where  $\alpha_1$ ,  $\alpha_{ij}$ ,  $\alpha_{ijk}$ , and  $\alpha_{ijkl}$  are the phenomenological Landau expression coefficients,  $v$  is the volume of the simulated system, and  $d^3x = dx_1dx_2dx_3$ .

The gradient energy in Eq. (2) is introduced through the gradients of the polarization field, i.e.,

$$F_{grad}(\partial P_i / \partial x_j) = \int_v \left[ \frac{1}{2} G_{ijkl} \frac{\partial P_i}{\partial x_j} \frac{\partial P_k}{\partial x_l} \right] d^3x, \quad (4)$$

where  $G_{ijkl}$  are the gradient energy coefficients with the property that  $G_{ijkl} = G_{klij}$ . For a multi-domain structure, the gradient energy represents the contribution of the ferroelectric domain wall to the total free energy and is only nonzero around domain walls.

Based on Khachaturyan's elastic theory,<sup>33</sup> the elastic energy term  $F_{elast}$  is given by

$$F_{elast}(P_i, \varepsilon_{ij}) = \int_v \left[ \frac{1}{2} c_{ijkl} (\varepsilon_{ij} - Q_{ijkl} P_k P_l) (\varepsilon_{kl} - Q_{klij} P_i P_j) \right] d^3x, \quad (5)$$

where  $\varepsilon_{ij}$  is the total strain and  $c_{ijkl}$  is the elastic stiffness tensor.  $Q_{ijkl}$  represents the electrostrictive coefficient.

The electric energy can be written as

$$F_{elec} = \int_v \left( -\frac{1}{2} \varepsilon_b \varepsilon_0 E_i^2 - E_i P_i \right) d^3x, \quad (6)$$

where  $\varepsilon_0$  is the vacuum permittivity and  $\varepsilon_b$  is the background relative dielectric permittivity. See Refs. 26, 31 and 34 for a discussion of the background dielectric constant. Please note that the electrostatic boundary conditions of the thin film superlattice structure are critical for the switching properties of the ferroelectric, which are relevant to applications. The work from Bratkovsky and Levanyuk,<sup>35,36</sup> Lukyanchuk *et al.*,<sup>37,38</sup> and Ahwuhalia and Srolovitz<sup>39,40</sup> show that the boundary conditions can strongly influence the domain morphology, domain size, domain wall width, and nucleation/switching properties. In this work, we assume there are no charged ionic/electronic defects compensating the polarization charges at these interfaces, and thus the polarizations across these interfaces are entirely determined by the competition among electrostatic, elastic, and interfacial energies

where  $F_{bulk}$ ,  $F_{grad}$ ,  $F_{elast}$ , and  $F_{elec}$  are the bulk chemical, gradient (or domain wall), elastic, and electrostatic energies, respectively.

The bulk chemical energy, for a centrosymmetric ferroelectric crystal, can be expanded by an eight-order Landau polynomial in polarization components

without explicitly imposing electrostatic boundary conditions while assuming the interfaces are coherent.

In this work, we assumed a homogeneous and isotropic dielectric constant of vacuum for both the BaTiO<sub>3</sub> and SrTiO<sub>3</sub> layers of the superlattice. There is minor difference between the simulated results obtained with  $\varepsilon_b = 1, 5$ , and 10. All the corresponding nonzero coefficients, including the Landau expression coefficients of the bulk free energy, the gradient energy coefficients, the electrostrictive and elastic coefficients, are listed here<sup>17,26,30</sup> for the BT layers:  $\alpha_1 = 4.124(T - 388) \times 10^5$ ,  $\alpha_{11} = -2.097 \times 10^8$ ,  $\alpha_{12} = 7.974 \times 10^8$ ,  $\alpha_{111} = 1.294 \times 10^9$ ,  $\alpha_{112} = -1.950 \times 10^9$ ,  $\alpha_{123} = -2.500 \times 10^9$ ,  $\alpha_{1111} = 3.863 \times 10^{10}$ ,  $\alpha_{1112} = 2.529 \times 10^{10}$ ,  $\alpha_{1122} = 1.637 \times 10^{10}$ ,  $\alpha_{1123} = 1.367 \times 10^{10}$ ,  $c_{11} = 1.78 \times 10^{11}$ ,  $c_{12} = 0.964 \times 10^{11}$ ,  $c_{44} = 1.22 \times 10^{11}$ ,  $Q_{11} = 0.10$ ,  $Q_{12} = -0.034$ ,  $Q_{44} = 0.029$ , for the ST layers:  $\alpha_1 = 2.6353[\coth(42/T) - 0.90476] \times 10^7$ ,  $\alpha_{11} = 1.696 \times 10^9$ ,  $\alpha_{12} = 1.373 \times 10^9$ ,  $c_{11} = 3.36 \times 10^{11}$ ,  $c_{12} = 1.07 \times 10^{11}$ ,  $c_{44} = 1.27 \times 10^{11}$ ,  $Q_{11} = 0.066$ ,  $Q_{12} = -0.0135$ ,  $Q_{44} = 0.0096$ , where  $c_{ij}$  and  $Q_{ij}$  are the Voigt notation for  $c_{ijkl}$  and  $Q_{ijkl}$  in SI units and  $T$  is in Kelvin. The pseudocubic lattice parameter for the BT and ST layers are set to be  $a_{BT} = 3.9994 \times 10^{-10} + 5.35386 \times 10^{-15} (T - 273)$ , and  $a_{ST} = 3.9043 \times 10^{-10} [(1 + 9.39) \times 10^{-6} (T - 273) + 1.97 \times 10^{-9} (T - 273)^2]$ , where  $T$  is in Kelvin.

In the simulation, we discretized the simulation cell as  $64 \Delta x_1 \times 64 \Delta x_2 \times N \Delta x_3$ , where  $\Delta x_1$ ,  $\Delta x_2$ ,  $\Delta x_3$  are grid spacing, and  $\Delta x_1 = \Delta x_2 = 1$  nm for the real space,  $\Delta x_3 = 0.5 a_{\text{substrate}}(\text{SrTiO}_3) \approx 0.2$  nm, and  $N = 2(m + n)$  for a BT<sub>*m*</sub>/ST<sub>*n*</sub> superlattice. Periodic boundary conditions are employed along the  $x_1$ ,  $x_2$ , and  $x_3$  axes. In order to simulate epitaxial strain relaxation conditions, different in-plane biaxial strain was introduced for each specific condition. The in-plane lattice parameter of the superlattice BT<sub>8</sub>/ST<sub>4</sub> with temperature can be found in Ref. 17. In this work, we just focus on the commensuratness of thin film/substrate interface, and the interfacial coherency between BT/ST layers is assumed to be fully commensurate.

Figures 1(a)–1(c) present the equilibrium domain structures of the superlattice BT<sub>8</sub>/ST<sub>4</sub> at room temperature under the three substrate mechanical constraint conditions considered without applying any electric field. The corresponding constraint strains on the ST layer and BT layer under the three considered conditions are listed in Table I. The in-plane

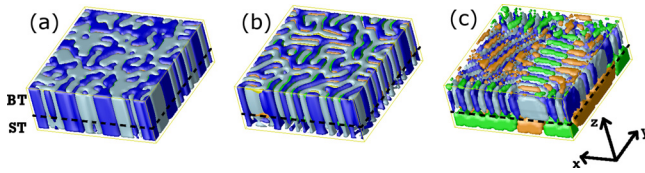


FIG. 1. (a)–(c) Simulated domain structures of a  $\text{BT}_8/\text{ST}_4$  superlattice under fully relaxed, partially relaxed, and fully commensurate mechanical boundary conditions, respectively. These domain structures are used as the starting structures to construct hysteresis loops. Each color represents a ferroelectric variant: blue/light blue represents tetragonal  $c^-/c^+$ , and green/orange represents orthorhombic  $[110]/[110]$ .

strain in the BT or ST layers can be expressed by  $\varepsilon_{\text{BT}/\text{ST}} = (a_{\text{sup}} - a_{\text{BT}/\text{ST}})/a_{\text{sup}}$ , where  $a_{\text{sup}}$  is the in-plane lattice parameter of the superlattice  $\text{BT}_8/\text{ST}_4$ . We note that the BT layer and ST layers are always coherent to each other. The constraint strains are from the underlying substrate in cases of fully commensurate, partially relaxed, and fully relaxed constraints, respectively. The domain structures shown in Fig. 1 were obtained by performing phase-field simulations that started from an initial paraelectric state with small random perturbations on polarizations. The ferroelectric phases/domains in the domain structures are illustrated by colors. Blue and light blue represent tetragonal phases of  $c^-$ :  $(0,0,-P_3)$  and  $c^+$ :  $(0,0,P_3)$ , respectively. Green represents orthorhombic phases of  $(P_1, P_2, 0)$  or  $(P_1, -P_2, 0)$  and orange represents orthorhombic phases of  $(-P_1, P_2, 0)$  or  $(-P_1, -P_2, 0)$  with  $P_1 = P_2$ .

It is seen that tetragonal  $c^+$  and  $c^-$  domains form “maze-like” domain structures with  $180^\circ$  ferroelectric domain walls for fully commensurate and partially relaxed cases, in both the ST and BT layers. Under the fully relaxed condition, which implies that the underlying substrate does not provide any in-plane constraint on the superlattice film, the ST layer consists of orthorhombic domains with in-plane polarizations while the BT layer is still composed of tetragonal domains with out-of-plane polarization. According to the phase diagram of ST thin films,<sup>41</sup> an in-plane orthorhombic phase is predicted under large in-plane constraint strains. The domain structure of Fig. 1(c) validates the prediction of ferroelectricity with the ST layer under a large in-plane constraint strain since the ST layer is subjected to  $\sim 1.7\%$  in-plane tensile strains under the fully relaxed condition. The ferroelectric tetragonal domains formed in the ST layer under both fully commensurate and partially relaxed conditions is attributed to the electrostatic interactions between the BT and ST layers as discussed in Ref. 17.

TABLE I. The lattice parameter of the  $\text{BT}_8/\text{ST}_4$  superlattice and the constraint strains in the ST layer and BT layer under different relaxation conditions.

$\text{BT}_8/\text{ST}_4$	Lattice parameter of $\text{BT}_8/\text{ST}_4$ superlattice at room temperature ( $a_{\text{sup}}$ )	Strain in BT layer = $(a_{\text{sup}} - a_{\text{BT}})/a_{\text{sup}}$	Strain in ST layer = $(a_{\text{sup}} - a_{\text{ST}})/a_{\text{sup}}$
Fully commensurate	3.905	-0.024	0.0
Partially relaxed	3.946	-0.014	0.0104
Fully relaxed	3.969	-0.008	0.016

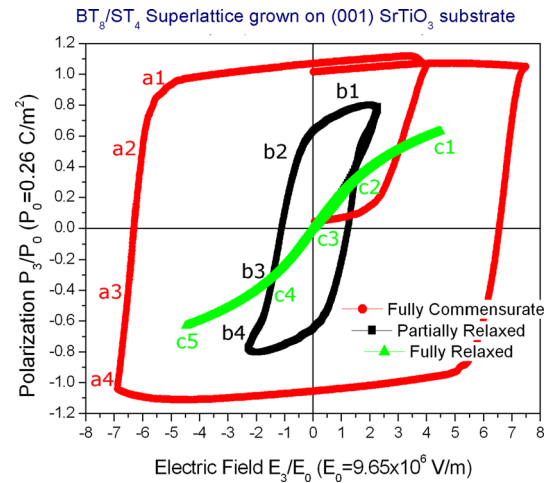


FIG. 2. The simulated ferroelectric hysteresis loops of a superlattice  $\text{BT}_8/\text{ST}_4$  under different conditions of mechanical constraint.

Figure 2 presents the calculated hysteresis loops for the superlattice under the three interfacial coherency conditions when an electric field is applied along the  $x_3$  axis. The hysteresis loop is obtained by plotting the normalized polarization ( $P/P_0$ ) versus normalized electric field ( $E/E_0$ ), where  $P_0 = |P_{\text{BT}}|_{T=25^\circ\text{C}} = 0.26 \text{ C/m}^2$ , and  $E_0 = \alpha_0 P_0 = 9.65 \times 10^6 \text{ V/m}$ , where  $\alpha_0 = |\alpha_1|_{T=25^\circ\text{C}}$ . The domain structures in Fig. 1 were the starting points of the hysteresis loops. From Fig. 2, it is seen that the lattice coherency between the superlattice film and the underlying substrate has a remarkable influence on the corresponding hysteresis loop, including both the coercive field and remanent polarization. As the mechanical constraint from the substrate is relaxed, both the remanent polarization and the coercive field decrease. The fully commensurate superlattice exhibits a square-like switching loop, with a high remnant polarization and a large coercive field; the partially relaxed superlattice shows a relative high remanent polarization with a dramatically reduced coercive field. It is interesting to notice that the switching loop of the fully relaxed superlattice becomes much slimmer with both small coercive field and remanent polarization.

To understand the switching behavior under relaxed conditions in the  $\text{BT}_8/\text{ST}_4$  superlattice, ferroelectric domain structures during the switching process were simulated. Figure 3 shows the evolution of the corresponding domain microstructures under fully commensurate and partially relaxed conditions. It should be borne in mind that since we did not consider any defect or inhomogeneous nucleation

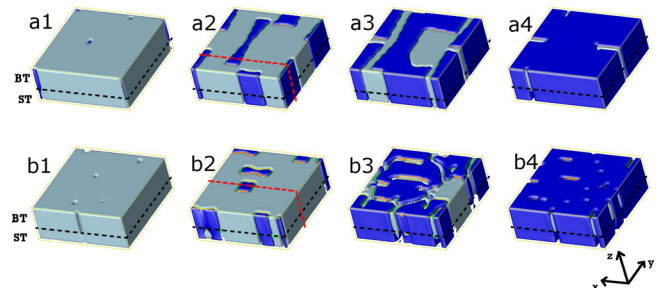


FIG. 3. The simulated morphology of ferroelectric domains in the  $\text{BT}_8/\text{ST}_4$  superlattice during the switching process: (a1)–(a4) under the fully commensurate condition, corresponding to point (a1)–(a4) in Fig. 2, and (b1)–(b4) under a partially relaxed condition, corresponding to point (b1)–(b4) in Fig. 2.

mechanism in our simulation, all of the switching processes did not end up in a single domain state. The switching loop of the fully commensurate superlattice is similar to that of BT. During the switching back process, the polarization decreases slowly and the domain structure has no significant change at first. A jump in polarization is observed at around  $5E_0$ , i.e.,  $4.825 \times 10^7$  V/m. We observe that the c-domain expanded quite rapidly with square-shaped  $180^\circ$  domain walls. Finally, the polarization is switched to the  $-z$  direction, and the polarization reaches saturation. Compared to the fully commensurate case, the coercive field of the partially relaxed case is dramatically reduced to approximately  $0.5E_0$ , which is about one tenth of the fully commensurate case.

The internal domain wall structures for the fully commensurate and partially relaxed cases are examined in Fig. 4. Figures 4(a) and 4(b) depict the vector distributions of the total polarization in the cross-section plane of the domain structure in Figs. 3(a2) and 3(b2), respectively (denoted by red dashed line in Fig. 3). It was found that the interfacial coherency influences the  $180^\circ$  domain wall width. From the variation of polarization in the  $z$  direction in the plane at the center of a BaTiO<sub>3</sub> layer (as shown in Figs. 4(c) and 4(d)), it is clear that the relaxation of the superlattice structure leads to the increase in the domain wall width in comparison with the case of fully commensurate. A Jacobi elliptic function  $P_z(x) = P_{zs} \text{SN}(x/\omega_0, m)$  is employed to approximate the simulation

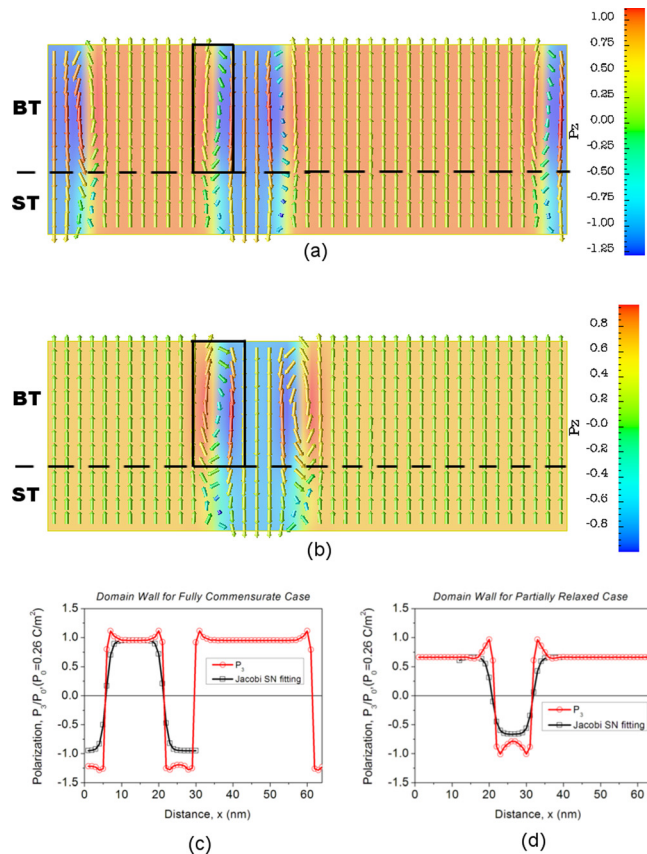


FIG. 4. (a) and (b) Simulated ferroelectric polarization vector distributions of the total polarization at the cross-section plane of the domain structure in Figs. 3(a2) and 3(b2), denoted by the red dashed line in Fig. 3. (c) and (d) The variation of polarization along the  $z$  direction in the plane at the center of a BaTiO<sub>3</sub> layer in Figs. 4(a) and 4(b), respectively. The black lines with squares at the calculated points are fits to simulated results.

results (the black lines in Figs. 4(c) and 4(d)),<sup>42</sup> where  $P_{zs}$  is the spontaneous polarization of a homogeneous system and  $\omega_0$  is a measure of the half width of the wall. Please note that as the simulation temperature (room temperature) is far below  $T_c$  for both cases, the Kittel-like domains are assumed in this work and a relative large  $m$  is chosen ( $m = 0.99$ ). The calculated width of the domain wall  $2\omega_0$  is  $\sim 2$  nm and  $\sim 3$  nm for the fully commensurate and partially relaxed cases, respectively. According to Ref. 43, the threshold field drops dramatically with an increase in the bulk wall width, which is consistent with the simulation results in Fig. 2. Interestingly, the ferroelectric domains for the fully commensurate and partially relaxed cases are very similar to the predicted “hard/soft domain” by Luk’yanchuka *et al.*<sup>37,38</sup> For the fully commensurate case, the compressive strain as large as 2.4% leads to a high  $T_c$  of  $\sim 1100$  K. As the simulation temperature (at room temperature) is far below  $T_c$ , a Kittel-like polarization profile is realized, and the domain structure with its physical properties behaves as “hard domains.” Because the  $T_c$  of the BT layer for the partially relaxed case is greatly reduced, a gradual polarization profile occurs and the domain structure is “softer.” An interesting observation of the out-of-plane polarization ( $P_z$ ) profiles is that they exhibit *higher values* near the domain wall (Figs. 4(c) and 4(d)). Note that electrostatic effects do not cause the polarization to increase near the domain wall, rather they cause the polarization away from the domain wall to decrease. At the domain walls, a vortex structure is formed and this electrostatic effect is greatly reduced, and eventually, a peak is observed in the polarization profile near the domain wall.

Notice that a fully relaxed BT<sub>8</sub>/ST<sub>4</sub> superlattice shows a paraelectric-like hysteresis loop. In contrast to paraelectric materials, a fully relaxed ferroelectric superlattice presents a P-E loop with a very high saturation polarization, but a small coercive electric field. The calculated slim switching loop for nano-scale ferroelectric superlattices is analogous to the “superparamagnetism” in magnetic nanoparticle systems. The calculated switching characteristics show that a fully relaxed superlattice has the potential to be relevant for energy storage applications<sup>44,45</sup> because of its high electric energy density and very low dielectric loss. Figures 5(a)–5(e) show both the domain morphology and vector plots of the cross-section

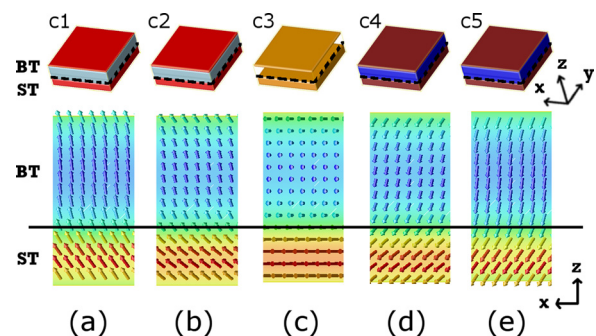


FIG. 5. (a)–(e) simulated single-domain structures and the cross-section vector plots of a fully relaxed superlattice during the switching process, corresponding to point (c1)–(c5) in Fig. 2. Light blue/blue represents  $c+/c$ -tetragonal phases, red and dark red represents monoclinic phases, and orange represents  $[1\bar{1}0]$  orthorhombic phases. There is only a small induced polarization in the BT layer in (c), which can be seen in the vector plots below.

plane during the switching process. It is interesting to observe a single ferroelectric polarization component switching during the domain switching. At saturation, a tetragonal/monoclinic phase was seen within BT/ST layers (Fig. 5(a)). With the decrease of the external electric field, the decrease of the polarization component  $P_3$  leads to the rotation of polarization vector in both the ST and BT layers (Fig. 5(b)). When the external electric field decreases to zero, an orthorhombic phase appears in both the ST and BT layers. The orthorhombic phase of the BT layer is induced to reduce the electrostatic energy of the system (Fig. 5(c)), because the orthorhombic phase is not a stable phase of a BT layer if the BT layer is not adjacent to a ST layer. Subsequent switching demonstrates a similar polarization rotating procession (Figs. 5(d) and 5(e)), and finally a linear hysteresis is generated.

In summary, the phase-field approach was applied to study the switching of a BT<sub>8</sub>/ST<sub>4</sub> superlattice under different interfacial coherency conditions. The ferroelectric domain configuration, the polarization orientations, and the movement of domain walls during the switching process were analyzed. Simulation results demonstrated that the mechanical constraint between the thin film and its underlying substrate can lead to significant changes in the shape of the ferroelectric hysteresis loop. Interfacial relaxation dramatically decreases the coercivity and remanence of the superlattice films.

This work was supported by the NSF under Grant No. DMR 1210588 (Chen and Gopalan), DMR-1234096 (Eom), DMR-1420620 (Schlom), and NSFC under the Grant No. 11174030 (Ma). The work at University of Wisconsin-Madison was supported by the Army Research Office under Grant No. W911NF-13-1-0486 (Eom). Wu was partially supported by a China Scholarship Council fellowship. The computer simulations were carried out on the LION and Cyberstar clusters at the Pennsylvania State University supported in part by NSF Major Research Instrumentation Program through grant OCI-0821527 and in part by the Materials Simulation Center and the Graduated Education and Research Services at the Pennsylvania State University.

- <sup>1</sup>J. C. Jiang, X. Q. Pan, W. Tian, C. D. Theis, and D. G. Schlom, *Appl. Phys. Lett.* **74**, 2851 (1999).
- <sup>2</sup>D. G. Schlom, J. H. Haeni, J. Lettieri, C. D. Theis, W. Tian, J. C. Jiang, and X. Q. Pan, *Mater. Sci. Eng., B* **87**, 282 (2001).
- <sup>3</sup>D. G. Schlom, L. Q. Chen, C. B. Eom, K. M. Rabe, S. K. Streiffer, and J. M. Triscone, *Annu. Rev. Mater. Sci.* **37**, 589 (2007).
- <sup>4</sup>D. G. Schlom, L. Q. Chen, X. Q. Pan, A. Schmehl, and M. A. Zurbuchen, *J. Am. Ceram. Soc.* **91**, 2429 (2008).
- <sup>5</sup>H. N. Lee, H. M. Christen, M. F. Chisholm, C. M. Rouleau, and D. H. Lowndes, *Nature London* **434**, 792 (2005).
- <sup>6</sup>H. Tabata, H. Tanaka, and T. Kawai, *Appl. Phys. Lett.* **65**, 1970 (1994).
- <sup>7</sup>T. Shimuta, O. Nakagawara, T. Makino, S. Arai, H. Tabata, and T. Kawai, *J. Appl. Phys.* **91**, 2290 (2002).
- <sup>8</sup>J. Kim, Y. Kim, Y. S. Kim, J. Lee, L. Kim, and D. Jung, *Appl. Phys. Lett.* **80**, 3581 (2002).
- <sup>9</sup>L. J. Kim, J. Kim, D. G. Jung, and J. Lee, *Appl. Phys. Lett.* **87**, 052903 (2005).
- <sup>10</sup>D. O'Neill, R. M. Bowman, and J. M. Gregg, *Appl. Phys. Lett.* **77**, 1520 (2000).

- <sup>11</sup>S. Rios, A. Ruediger, A. Q. Jiang, J. F. Scott, H. Lu, and Z. Chen, *J. Phys.: Condens. Matter* **15**, L305 (2003).
- <sup>12</sup>A. Q. Jiang, J. F. Scott, H. B. Lu, and Z. H. Chen, *J. Appl. Phys.* **93**, 1180 (2003).
- <sup>13</sup>J. B. Neaton and K. M. Rabe, *Appl. Phys. Lett.* **82**, 1586 (2003).
- <sup>14</sup>K. Johnston, X. Y. Huang, J. B. Neaton, and K. M. Rabe, *Phys. Rev. B* **71**, 100103(R) (2005).
- <sup>15</sup>S. Lisenkov and L. Bellaiche, *Phys. Rev. B* **76**, 020102(R) (2007).
- <sup>16</sup>D. A. Tenne, A. Bruchhausen, N. D. Lanzillotti-Kimura, A. Fainstein, R. S. Katiyar, A. Cantarero, A. Soukiasian, V. Vaithyanathan, J. H. Haeni, W. Tian, D. G. Schlom, K. J. Choi, D. M. Kim, C. B. Eom, H. P. Sun, X. Q. Pan, Y. L. Li, L. Q. Chen, Q. X. Jia, S. M. Nakhmanson, K. M. Rabe, and X. X. Xi, *Science* **313**, 1614 (2006).
- <sup>17</sup>Y. L. Li, S. Y. Hu, D. Tenne, A. Soukiasian, D. G. Schlom, L. Q. Chen, X. X. Xi, K. J. Choi, C. B. Eom, A. Saxena, T. Lookman, and Q. X. Jia, *Appl. Phys. Lett.* **91**, 252904 (2007).
- <sup>18</sup>D. A. Tenne, H. N. Lee, R. S. Katiyar, and X. X. Xi, *J. Appl. Phys.* **105**, 054106 (2009).
- <sup>19</sup>S. Gariglio, N. Stucki, J.-M. Triscone, and G. Triscone, *Appl. Phys. Lett.* **90**, 202905 (2007).
- <sup>20</sup>A. I. Khan, P. Yu, M. Trassin, M. J. Lee, L. You, and S. Salahuddin, *Appl. Phys. Lett.* **105**, 022903 (2014).
- <sup>21</sup>R. Ranjith, B. Kundys, and W. Prellier, *Appl. Phys. Lett.* **91**, 222904 (2007).
- <sup>22</sup>S.-J. Chiu, Y.-T. Liu, H.-Y. Lee, G.-P. Yu, and J.-H. Huang, *Thin Solid Films* **539**, 75 (2013).
- <sup>23</sup>N. Ortega, A. Kumar, O. A. Maslova, Yu. I. Yuzyuk, J. F. Scott, and R. S. Katiyar, *Phys. Rev. B* **83**, 144108 (2011).
- <sup>24</sup>N. Ortega, A. Kumar, J. F. Scott, D. B. Chrisey, M. Tomazawa, S. Kumari, D. G. B. Diestra, and R. S. Katiyar, *J. Phys.: Condens. Matter* **24**, 445901 (2012).
- <sup>25</sup>O. Auciello, J. F. Scott, and R. Ramesh, *Phys. Today* **51**(7), 22–27 (1998).
- <sup>26</sup>P. W. Wu, X. Q. Ma, Y. L. Li, V. Gopalan, and L. Q. Chen, *Appl. Phys. Lett.* **100**, 092905 (2012).
- <sup>27</sup>A. Artemev, *Appl. Phys. Lett.* **103**, 132912 (2013).
- <sup>28</sup>M. Dawber, N. Stucki, C. Lichtensteiger, S. Gariglio, P. Ghosez, and J. M. Triscone, *Adv. Mater.* **19**, 4153 (2007).
- <sup>29</sup>D. Lee, R. K. Behera, P. P. Wu, H. X. Xu, Y. L. Li, S. B. Sinnott, S. R. Phillpot, L. Q. Chen, and V. Gopalan, *Phys. Rev. B* **80**, 060102(R) (2009).
- <sup>30</sup>Y. L. Li, S. Y. Hu, D. Tenne, A. Soukiasian, D. G. Schlom, X. X. Xi, K. J. Choi, C. B. Eom, A. Saxena, T. Lookman, Q. X. Jia, and L. Q. Chen, *Appl. Phys. Lett.* **91**, 112914 (2007).
- <sup>31</sup>Y. Zheng and C. H. Woo, *Appl. Phys. A- Mater.* **97**, 617 (2009).
- <sup>32</sup>D. C. Ma, Y. Zheng, and C. H. Woo, *Acta Mater.* **57**, 4736 (2009).
- <sup>33</sup>A. G. Khachatryan, *Theory of Structural Transformations in Solid* (Wiley, New York, 1983).
- <sup>34</sup>A. K. Tagantsev, *Ferroelectrics* **375**, 19 (2008).
- <sup>35</sup>A. M. Bratkovsky and A. P. Levanyuk, *Phys. Rev. Lett.* **94**, 107601 (2005).
- <sup>36</sup>A. M. Bratkovsky and A. P. Levanyuk, *Phys. Rev. Lett.* **86**, 3642 (2001).
- <sup>37</sup>F. De Guerville, I. Luk'yanchuk, L. Lahoche, and M. El Marssi, *Mater. Sci. Eng. B* **120**, 16 (2005).
- <sup>38</sup>V. A. Stephanovich, I. A. Luk'yanchuk, and M. G. Karkut, *Phys. Rev. Lett.* **94**, 047601 (2005).
- <sup>39</sup>R. Ahluwalia and D. J. Srolovitz, *Phys. Rev. B* **76**, 174121 (2007).
- <sup>40</sup>N. Ng, R. Ahluwalia, and D. J. Srolovitz, *Phys. Rev. B* **86**, 094104 (2012).
- <sup>41</sup>Y. L. Li, S. Choudhury, J. H. Haeni, M. D. Biegalski, A. Vasudevarao, A. Sharan, H. Z. Ma, J. Levy, V. Gopalan, S. Trolier-McKinstry, D. G. Schlom, Q. X. Jia, and L. Q. Chen, *Phys. Rev. B* **73**, 184112 (2006).
- <sup>42</sup>I. A. Luk'yanchuk, L. Lahoche, and A. Sené, *Phys. Rev. Lett.* **102**, 147601 (2009).
- <sup>43</sup>S. Choudhury, Y. L. Li, N. Odagawa, A. Vasudevarao, L. Tian, P. Capek, V. Dierolf, A. N. Morozovska, E. A. Eliseev, S. Kalinin, Y. Cho, L.-Q. Chen, and V. Gopalan, *J. Appl. Phys.* **104**, 084107 (2008).
- <sup>44</sup>B. Chu, X. Zhou, K. Ren, B. Neese, M. Lin, Q. Wang, F. Bauer, and Q. M. Zhang, *Science* **313**, 334 (2006).
- <sup>45</sup>J. Li, S. Seok, B. Chu, F. Dogan, Q. Zhang, and Q. Wang, *Adv. Mater.* **21**, 217 (2009).